Experimental Visualization of gas-assisted injection long bubble in a tube

Cheng-Hsing Hsu[1], Kuang-Yuan Kung[2*], Po-Chuang Chen[3] ,and Shu-Yu Hu[1]
[1] Department of Mechanical Engineering Chung-Yuan Christian University.
[2*] Department of Mechanical Engineering Nanya Institute of Technology.
414 Sec. 3 Chung Shang East R. Chung Li 320 TAIWAN.
[3] Nuclear Fuels and Materials Division, Institute of Nuclear Energy Research
ky.kung@msa.hinet.net http://www.nanya.edu.tw

Abstract:- A long bubble-driven fluid flow in a circular tube is visualized by an optical method. A pressurized airflow was injected into an 8 mm I.D. and 1,500 mm long horizontally placed glass tube filled with silicon oil to produce a long bubble in the tube. The images were analyzed by two-value calculation and a thinning process to extract the contour of the bubble front. Data points on the contour were then deduced to undergo a regression curve fitting. The results show a good verification of the theoretically derived non-dimensional contour equation. The deduced penetration speed indicates that the speed is increasing downstream due to the decreasing fluid slug in the tube. The experimental results shows the theoretical bubble profile can be introduced to the simulation study to reduce the calculating time, the ratio (λ) of the bubble width to the diameter of the circular tube. The theoretical bubble profile is more precise in a lower λ value than in a higher one.

Keyword:- Long bubble, Contour equation, Two-phase flow, Correlated number, Optical method

1 Introduction

Using long bubble to assist manufacture or medical processes is common in various industries, such as gas-assisted injection molding, bio-mechanic process and medical treatment process, etc. Particularly, the information about the expelled fluid flow in front of the bubble and the contour of the bubble front are of great interests in the simulating processes.

Using the fundamental dynamic equations of the bubble by some theoretical or experimental deduced empirical equations can practically simplify simulation procedures. The flow patterns, and the migration of stagnation point and the influence of the inertia forces on the flow field are presented in this study. The impacts of the bubble size on the flow field draw a great interest of many researchers [2, 10-12]. Fairbrother and Stubbs [1] first studied the penetration of a long bubble in a tube. The empirical formula between the fractional coverage is obtained.

Sabry [3] used to simulate a two phase flow of natural gas and condensed droplets through a convergent-divergent nozzle of the gas-dynamic equations. A modified nucleation theory is used to estimate the nucleation coefficient and the nucleation rate. A numerical technique is used to solve the governing equations. The increase of both initial pressure and correction coefficient leads to a rapid appearance of sub-cooling, the process becomes more non-equilibrium and the zone of spontaneous condensation is shifted downstream towards a region with larger sub-cooling. The increase of both initial pressure and the correction coefficient besides the decrease of condensation coefficient cause a rapid decay of shock condensation, rapid growth of droplets in the initial stage of condensation and slower further downstream. The results obtained here show that increasing the correction coefficient as well as increasing the low initial pressure delayed the zone of condensation towards the nozzle exit, while at moderate initial pressure the observed shock condensation moves towards the nozzle throat.

C.H. Hsu et.al. [2] numerically studied the Long Gas Bubble Front. Taylor [4] presented three fluid flow patterns, two kinds of re-circulating flows with a low capillary number, and a by-pass flow with high capillary number. Bretherton [5] developed a theoretical formula relating the fractional coverage and the pressure drop across the bubble. Goldsmith and Mason [6] visualized the flow pattern, the coating thickness and the shape of the bubble front.

M. AFSHAR [7] used a new model for numerical simulation of two-phase flows in complex geometries is presented which is the first step in developing numerical simulation models for boiling heat transfer in complex geometries. The complexity

of turbulence and two-phase flows exists in this problem and therefore, logical, convenient simplifications were made to solve the problem. A finite-volume based finite-element model is developed which resolved the difficulties for solving turbulent, single-phase flows in complex geometries. Also, a modified k-ε model is utilized for the solution of turbulent, two-phase bubbly flows. Since in many industrial applications, the flow is fully-developed, this problem is solved for this region. Considering the complexity of the problem, the results generated by numerical simulation are encouraging, and follow the data obtained in the corresponding experimental investigation of bubbly two-phase flows. Nevertheless, much effort is needed in modeling and numerical simulation methods to develop a sophisticated industrial tool.

Hassan [8] used a new experimental set-up was used to analyze the characteristics of the bubbles rising in water and three different concentrations of xanthene's gum solutions for higher Reynolds number. The bubble size, bubble rise velocity, and bubble trajectory were measured using a combination of non-intrusive-high speed photographic method and digital image processing. In xanthene's gum solutions, small bubbles experience less horizontal motion than that in water. Drag coefficients for air bubbles at higher Reynolds number are reported. It is seen that the experimental drag coefficient increases with the increase in xanthene's gum concentration corresponding to the same bubble volume. This experimental data of drag coefficient increases with the increase in xanthene's gum concentration for corresponding bubble volume. The relationship between Cd-Re for different concentration xanthene's gum solutions showed acceptable results with the available analytical and experimental studies in the literature with a wide range of Reynolds numbers. The bubble rise characteristics, namely, bubble velocity, trajectory and drag coefficient produced acceptable and consistent results.

Cox [9-10] extended Taylor's experiment and proposed a numerical solution of the momentum equation. The study indicated that at higher capillary number the fractional coverage approaches an asymptotic value $m = 0.6$, estimated by Taylor. Cox also developed an empirical equation of the bubble profile, verified the existence of the two flow patterns and found that the velocity in the fluid about 1.5-times inner diameter before the bubble tip was conformed to the Poiseuille flow. In the Hele-Shaw cell model, Pitts [26] reported a theoretical bubble shape equation for λ smaller than 0.77.

Mavridis et al. [11] studied the process about the polymer melts front, and compared the melt front shape between Newtonian and non-Newtonian fluids for two-dimensional and axi-symmetric cases. Schwartz et al. [12] found that λ is the function of the capillary number only, which agreed with Taylor. Kolb and Cerro [13] observed the bubble in a square tube filled with a Newtonian fluid, and found that the fractional coverage also reaches an asymptotic value $m = 0.64$ with increasing capillary number.

Poslinski and Stokes [14] studied the displacements of two silicon pastes in a circular tube to show the property of shear thinning of the fluid in the gas-assisted injection process. The parameter λ varies with the capillary number, and reaches a constant under higher capillary number or a critical pressure.

Brannock and Kubie [15] investigated the rising speed of long bubble with influence of the vertical sinusoidal motion in a vertical pipe with sealed top. They indicated that the rising speed was decreasing with increasing vertical acceleration or the smaller tube's diameter. Later, Kubie [16] continued his study on horizontal sinusoidal pipe motion but the result was quite different with their previously studied. The rising speed was increasing with higher acceleration, amplitude and smaller tube's diameter. The distortion of the bubble shape in an oscillating pipe was found in the study. Polonsky et al. [17] studied the velocity fields ahead of Taylor bubble in a vertical pipe, and the inception of negative velocity and the location of the onset of the reversed flow were observed in their measurement results.

Huzyak and Koelling [18] studied the influence on fractional coverage by experiments included Newtonian and visco-elastic fluids. They indicated that fractional coverage is only related to the capillary number for the Newtonian fluid but is the function of both the capillary number and the inner diameter of the tube for the visco-elastic fluid. Later, Gauri and Koelling [19] extended their experiments to measure the flow field near the bubble tip by using PTV (Particle Tracking Velocimetry) technique and verified the two typical flow patterns suggested by Taylor.

Giavedoni and Saita [20] studied the influence of capillary number and Reynolds number on the film thickness and verified the flow patterns suggested by Taylor for two-dimensional and axi-symmetric cases by using finite element method. They also noticed another recirculation pattern in the two-dimensional case. Later, Giavedoni and Saita [21] extended their study and discussed the influence of inertia force and capillary number on trailing meniscus shape of a long bubble. They also reported the flow

pattern.

For a rectangular tube, Wong et al. [22-23] performed an experiment and a theoretical analysis, and proposed a shape equation of the bubble front similar to Pitts' work. Liao and Zhao [24] presented theoretical analysis of a Taylor bubble (an elongated bubble) moving in vertical mini triangular and square channels, they transported the bubble profile to hydraulic diameter in the theoretical procedure by assuming the contact angle of the liquid at the channel wall is zero. They reported that the drift velocities in the triangular channel substantially higher than that in the square channel under the same hydraulic diameter. Kamişli [25] studied the fractional coverage and bubble width as a function of capillary number for quasi three-dimensional flow.

However, the study of the effects of the ratio of bubble width to the half width of confined fluid using a theoretical bubble's profile is absent. In the present work, the flow patterns in front of a semi-infinite gas bubble in numerical analysis in the geometry of parallel flat plate previously considered by Reinelt and saffman [26] were computed. The streamlines obtained demonstrate how the flow field changes when λ (the ratio of a asymptotic bubble width to the half width of confined fluid) is varied and evidently exist recirculation flow and the migration of stagnation point.

In the present study, the visualization was made in a tube with 12-mm outer diameter and 8-mm inner diameter. The shape equation of the bubble front, the bubble penetration speed and the driving pressure were obtained. The identified empirical equation of the bubble contour can be trusted as the boundary condition in the fluid flow simulation work to reduce the load of computing the driven flow field and the interface of two fluids simultaneously.

2 Apparatus and Experiment Parameters

Fig. 1 is the related coordinates and dimensions of the bubble in the tube filled with the test fluids. Where θ, r, z, R_b and R_0 are the angle between the bubble axis and the contour point position vector, radial and axial coordinates, asymptotic bubble radius and tube inner radius respectively.

A pressurized airflow was injected into a tube which filled with the test fluid. The injection air caused the test fluid to move out and form a long bubble finger. The schematic diagram of the apparatus is shown in Fig. 2. A 1500 mm long and 8 mm I.D. glass tube was used in the present experiment.

Two black-and-white CCD cameras, an image separator (4 images maximum/window) and a Matrox Meteor-II frame grabber were used to grab images (sampling at 30 frames/second) of the bubble front and monitored the pressure variation at the inlet of the tube. The software, Matrox Inspector, was used to control the grabber and to process the images, such as two-value calculating, contour-line thinning, and close computing, of the bubble.

The software, Matrox Inspector, is used to control the grabber and to process the images, such as two-value calculating, contour-line thinning, and close computing, of the bubble.

The light source was four light bulbs which located around the CCD cameras to provide sufficient light. In order to avoid the influence of surrounding light on the image grabbing process, an opaque object was used in the experimental study. A pressure transducer was used to measure and monitor the inlet pressure of the bubble. The experiment parameters are shown in the table 1 and the properties of the test fluids are supplied at 25 ℃.

	Injection Gas	Test Fluid (Silicon Oil)			
	Air	100 CS	350 CS	1,000 CS	10,000 CS
Specific Gravity (tolerance)	1.23E-3	0.964 (0.960-0.970)	0.968 (0.965-0.975)	0.97 (0.965-0.975)	0.974 (0.970-0.980)
Surface Tension (dyne/cm)		20.9	21.1	21.2	21.5
Kinematic Viscosity (cm^2/s)		1 (1±0.05)	3.5 (3.5±0.17)	10 (10±0.5)	100 (100±5)
Dynamic Viscosity (dyne*s/cm^2)	1.79E-4	0.964	3.388	9.7	97.4
Ratio of Air's Dynamic Viscosity	1	1.86E-4	5.28E-5	1.85E-5	1.84E-6

Table 1

Pitts (1980) proposed a contour equation of the bubble front based on a presumption $R\,\mathrm{Sin}\theta =$ constant value in the Hele-Shaw cell case. R is the radius of the curvature of the bubble contour. Following the concept from Pitts (1980), one can get the contour equation of the bubble in circular coordinates as

$$\mathrm{Cos}\left(-\frac{\pi r}{2R_b}\right)\exp\left(-\frac{\pi z}{2R_b}\right)=1 \qquad (1)$$

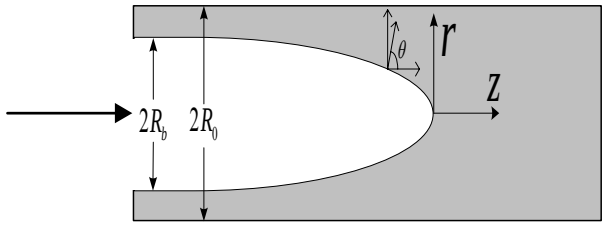

Fig. 1 Schematic of Bubble and Coordinates

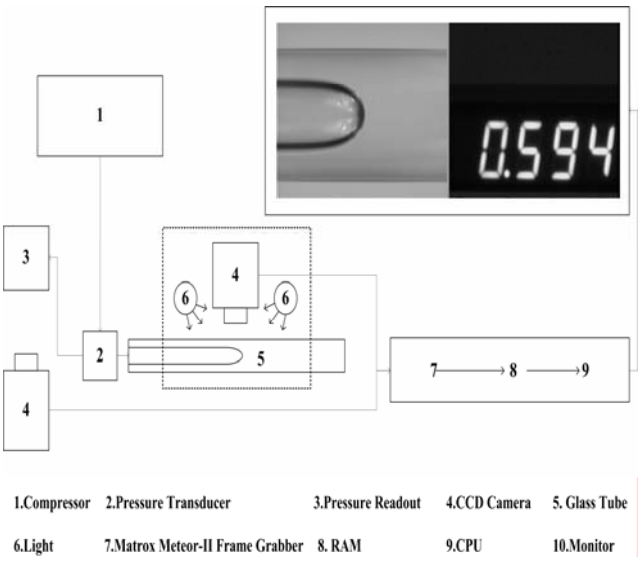

Fig. 2 A schematic diagram of the experimental setup

In order to simplify the problem, those parameters are defined as follow

$$r^*=\frac{r}{\mathrm{R}_0},\ z^*=\frac{z}{\mathrm{R}_0},\ \lambda=\frac{\mathrm{R}_\mathrm{b}}{\mathrm{R}_0},$$

Rearranging the equation (1), a dimensionless form is written as

$$r^*=\pm\frac{2\lambda}{\pi}\mathrm{Cos}^{-1}\left[\exp\left(\frac{\pi z^*}{2\lambda}\right)\right] \qquad (2)$$

Images of the present experiment are correlated based on the form of the equation (2) to verify the accuracy of the contour equation and the similarity of the shape of the bubble front. The form of the bubble front is assumed as

$$r^*=\pm A_1\lambda\mathrm{Cos}^{-1}\left[\exp\left(\frac{A_2 z^*}{\lambda}\right)\right], \qquad (3)$$

This is a nonlinear regression analysis equation. The exact values of A_1 and A_2 are $2/\pi$ and $\pi/2$, respectively.

The tube was initially filled with the test fluid and the experiments were conducted with several inlet driving pressures. The experimental data were recorded from 0 cm to 110 cm with increments of 10 cm. The software, Matrox Inspector, was introduced into the images handling process. The images were captured and processed through two-value calculating (based on gray level), contour line thinning (erosion), and close computing to obtain better image quality for average speed and curve fitting calculations. In each recording position, the image recording processes were repeated three times under the same experimental conditions.

(1)

Gas Bubble Test Fluid

Then the recorded data were averaged to reduce experimental error under the same recording position and experimental setting. As mentioned by Cox (1964), the width of the bubble front reached an asymptotic width at 1.5-diameter ($3R_0$) downstream of the bubble tip, so we used the width from the images to correlate the bubble profile and calculate λ. The data points of the bubble front contour were extracted from the images to obtain correlated curves by the regression processes. Then, the bubble velocity, driving pressure, bubble front contour and the nonlinear regression analysis results were obtained and are presented in the following section.

3 Results and Discursions

The original images of the bubble front and the processed contours are shown in Fig. 3. Fig.4 is bubble front speed versus the recording position. The bubble front speed is calculated from images according to the difference in position between adjacent frames and the sampling time.

Deacha [30], used conventional system identification requires sensor(s) to record input(s) and output(s) of a system. Under some circumstances, hazardous environment and/or confined area for instance, sensor installation may be difficult or even not possible. Deacha [30], proposes a new approach to system identification via image processing techniques mat permit non-intrusive and remote identification. One (or more) camera(s) can be an

alternative to conventional sensors. Recorded images contain a great deal of useful dynamical information of the system. Details of information extraction from images are presented in this paper. For linear models, conventional identification techniques based on regression analysis are applied. For nonlinear models, the adaptive tabu search (ATS), one of the AI search techniques, is employed. The approach has been tested against the cart-plus-pendulum (CPP) system, and the vibrating tube system (VTS), respectively. Practical results have been achieved with high satisfaction.

The position is measured from the gas inlet to show the location of the bubble tip along the glass tube. Unlike some previous studies such as Kamişli and Ryan (1999, 2001a), we mounted a valve on the outlet end to control the velocity near the constant. The outlet was fully open to allow the test fluid to move out as the experiment proceeded in the present study, thus the velocity is not a constant value. The setting results in the bubble speed varying during the experiment. In general, the bubble speed increases as the bubble moves toward the outlet.

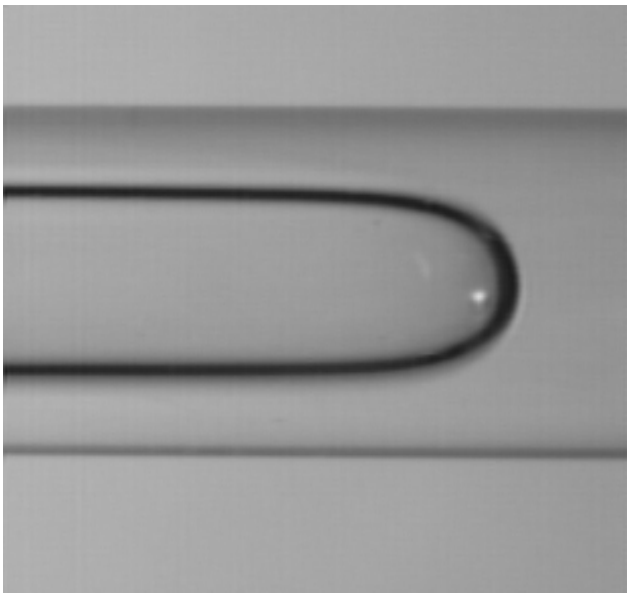

(a) Original Image

(b) Two-value Calculation

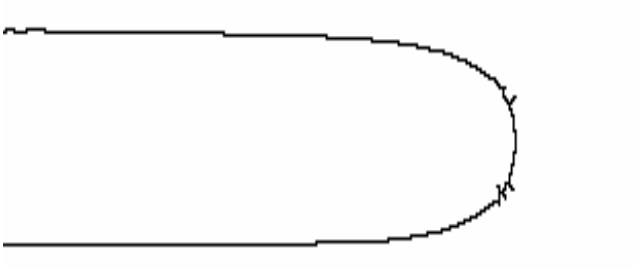

(c) Contour Thinning Computation

Fig. 3 The Processes of Image Processing

The resistance and the inertia of the fluid slug decrease when more and more amount of the fluid is expelled from the outlet.

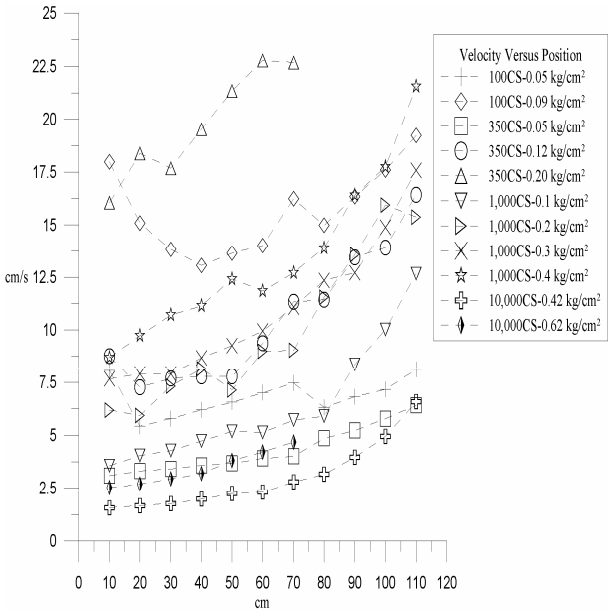

Fig. 4 Bubble Front Velocity Variations Versus Bubble Positions

The bubble speed decreases then increases when the viscosity of the test fluid is smaller and driven pressure is higher. The area where the bubble speed decreases may be the transient state of a suddenly higher inlet pressure. The bubble speed is higher at higher inlet pressure for the same test fluid. The distribution of the pressure versus position is presented in Fig. 5.

The inlet pressure decreases with the increasing bubble position, then nearly reaches a constant value. The region of the decreasing pressure is extended

with larger inlet pressure for the same test fluid, and the phenomena are easier found in the lower viscosity of the fluid as showed in Fig. 5(b).

Those results also verified the result in which the speed of the bubble is decreasing and then increasing in Fig. 4. The dimensionless contour of the bubble front and the relative dimensionless coordinates of the points on the contour were deduced from the images. For instance, five dimensionless shapes of the bubble front with five different values of λ are shown in Fig. 6. It implies that

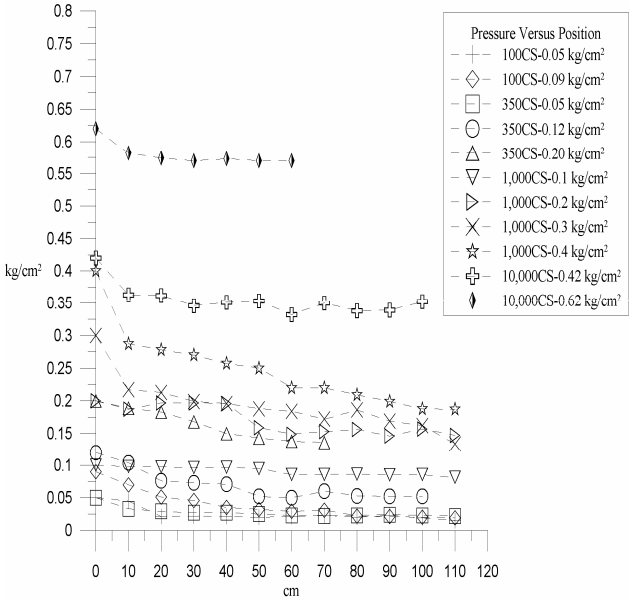

Fig. 5(a) Pressure Versus Position for Four Kinds of Test Fluids

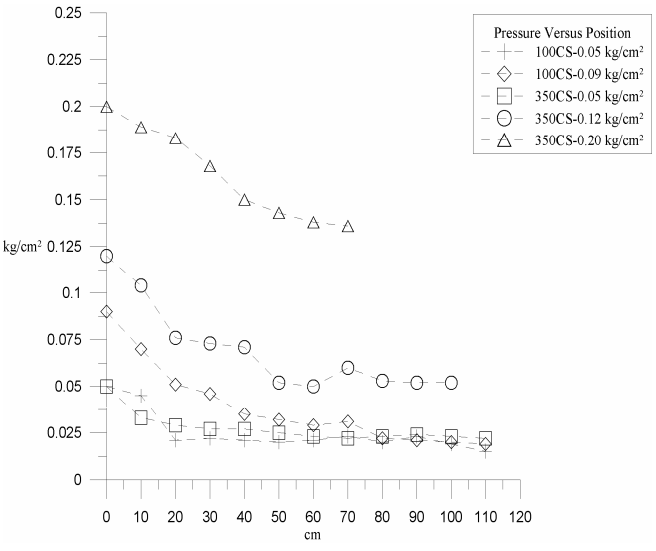

Fig. 5(b) Pressure Versus Position for Two Kinds of Test Fluids

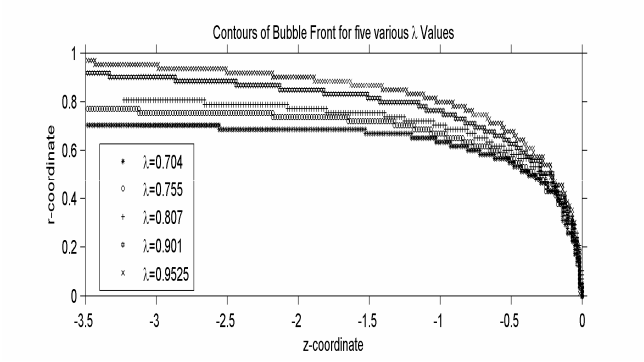

Fig. 6 Contours of Bubble Front for five various λ Values

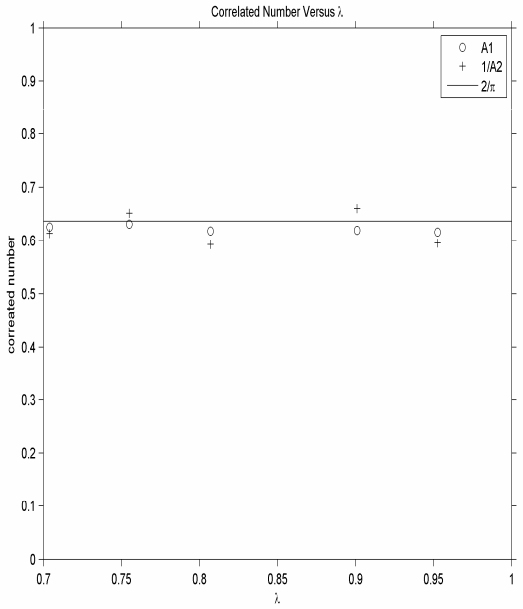

Fig. 7 Correlated Number Versus Lambda

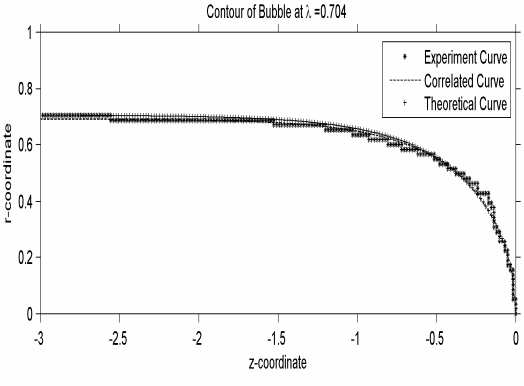

Fig. 8 Contour of the Bubble Front at λ= 0.704

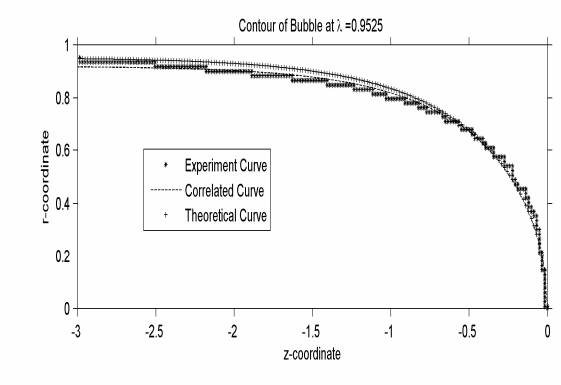

Fig. 9 Contour of the Bubble Front at λ= 0.9525

the shape of the bubble front is related to the λ, and the asymptotic radius of the bubble front, after the 1.5-diameter ($3R_0$) downstream of the bubble tip, gets larger with higher λ. Those results show the asymptotic radius in higher λ value (about λ >0.77) could not be observed in the range of 1.5-diameter ($3R_0$) downstream of the bubble tip. Farther than 1.5-diameter of the bubble tip, the asymptotic radius could be found.

Those results show that the usability of the empirically deduced bubble profile is limited under the condition of lower λ value (about λ <0.77). This result is similar to the previous study result of Pitts (1980). Although the asymptotic radius in higher λ value is not fund in 1.5-diameter of the bubble tip, for convenience, the all present λ value was calculated base on the 1.5-diameter of the bubble tip. Then we took the data into regression analysis to compare with the empirical deduced bubble profile.

Fig. 7 shows the nonlinear regression analysis results of correlated numbers, A_1 and $1/A_2$, from equation (3). The results of the correlated numbers are close to the theoretical value 2/π for various λ. Although the analysis results in higher λ value region seen to meet the empirical equation, the asymptotic radius in this region is not found. Thus, the empirical equation is little deviated to describe the real bubble contour.

When the location in z^* axis of asymptotic radius in higher λ value region is identified, it may be used to modify the empirical equation and push the usability region up to a higher λ value case. The dimensionless contour points from the images, the correlated dimensionless contour curves and the theoretical curve are shown in Fig.8 and Fig. 9 on the basis of case one, and the values of λ equal 0.704 and 0.9525 respectively.

The correlated curves are very close to the experimental and theoretical ones, and the experimental curve is very close to the theoretical one. As the λ value increases, the deviation of the experimental curve to the theoretical one also increases. This verifies that the theoretical bubble profile is more precise in a lower λ value than in a higher one.

4 Conclusions

A long bubble-driven fluid flow in a circular tube is visualized by an optical method. This provides good verification to the theoretically derived non-dimensional contour equation,

$$r^* = \pm \frac{2\lambda}{\pi} \cos^{-1}\left[\exp\left(\frac{\pi z^*}{2\lambda} \right) \right].$$

This equation is based on two presumptions, the bubble front curvature equation ($R \operatorname{Sin}\theta$ = constant value) and the similarity of the bubble shape in expelling a fluid.

The stagnant range decreases as the λ increases, and it also verifies the real physical phenomenon of zero velocity at the far downstream. As the Reynolds number increases, the fluids near the bubble tip expelled to move toward the centerline and the velocities increase in recirculation flow region. But the increasing of Reynolds number does not have notable effect on the flow field in complete bypass flow region.

The experimental results shows the theoretical bubble profile can be introduced to the simulation study to reduce the calculating time. As the λ value increases, the deviation of the experimental curve to the theoretical one also increases. The theoretical bubble profile is more correct in a lower λ value than in a higher one.

Nomenclature:

R : Radius of the tube
m : The factor of the fractional converge
$_P$: Pressure in the fluid expelled by bubble
r : The radial direction in coordinate system
$\vec{u}$: The velocity of the fluid expelled by bubble
z : The axial direction in coordinate system
λ : The ratio of asymptotic bubble width to radius of circular tube
Θ: The angle between the bubble axis and the contour point position vector
*: Dimensionless form

Acknowledgment

The present investigation was supported by National Science Council of Taiwan under granted NSC-97-2221-E-253-014-

References:

[1] Fairbrother, F.P. and Stubbs, A.E., Studies in electroendosmosis. Part VI. The bubble tube method of measurement, *J. Chem. Sci.*, Vol. 1, 1935, pp.527-529.

[2] C.H. Hsu, P.C. Chen, K.Y. Kung, G.C. Kuo Pressure Field in Front of Long Gas Bubble in a Fluid Filled Channel, *WSEAS TRANSACTIONS ON MATHEMATICS*, Vol. 5, 2006, pp.231-235.

[3] N. M. S. HASSAN, M. M. K. KHAN, AND M. G. RASUL, A Study of Bubble Trajectory and Drag Co-efficient in Water and Non-Newtonian Fluids, *WSEAS TRANSACTIONS on FLUID MECHANICS*, Vol. 3, Issue 3, 2006, pp.261-270.

[4] Taylor, G.I., Deposition of a viscous fluid on the wall of a tube, *J. Fluid Mech.*, Vol. 10, 1961, pp.161-165.

[5] Bretherton, F.P., The motion of long bubbles in tubes, *J. Fluid Mech.*, Vol.10, 1961, pp.166-188.

[6] Goldsmith, H.L. and Mason, S.G., The movement of single large bubbles in closed vertical tubes, *J. Fluid Mech.*, Vol.14, 1962, pp. 42-58.

[7] M. AFSHAR, Numerical Simulations of Turbulent, Two-Phase Flows in Complex Geometries, *Proceedings of the 3rd IASME/WSEAS Int. Conf. on HEAT TRANSFER, THERMAL ENGINEERING AND ENVIRONMENT, Corfu, Greece*, 2005, pp.338-343.

[8] T. I. Sabry, J. Huhn, N. H. Mahmoud, Mofreh H. Hamed and A. A. El-Batawy, *Proceedings of the WSEAS/IASME International Conference on Heat and Mass Transfer, Miami, Florida, USA*, 2006,pp.24-32.

[9] Cox, B.G., On driving a viscous fluid out of a tube, *J. Fluid Mech.*,Vol.14, 1962, pp.81-96.

[10] Cox, B.G., An experimental investigation of the streamlines in viscous fluids expelled from a tube, *J. Fluid Mech.*, Vol.20, 1964, pp.193-200.

[11] Mavridis, H. and Hrymak, A. N. and Vlachopoulos, J., Finite element simulation of

fountain flow in injection molding, *Polym. Eng. Sci*., Vol.26, 1986, pp.449-454.

[12] Schwartz, L.W., Princen, H.M. and Kiss, A.D., On the motion of bubbles in capillary tubes, *J. Fluid Mech.*, Vol.172, 1986,pp.259-275.

[13] Kolb, W.B. and Cerro, R.L., Coating the inside of a capillary of square cross section, *Chem. Eng. Sci.*, Vol.46, 1991, pp.2181-2195.

[14] Poslinski, A.J. and Stokes, V.K. Gas-assisted displacement of a viscous liquid in tube., *ANTEC*, 1993,pp.68-73.

[15] Brannock, D., Kubie, J., Velocity of long bubbles in oscillating vertical pipes, *Int. J. Multiph. Flow*, Vol.22, 1996, pp.1031-1034.

[16] Kubie, J., Velocity of long bubble in horizontally oscillating vertical pipes, *Int. J. Multiph. Flow*, Vol.26, 2000, pp.339-349.

[17] Polonsky, S., Shemer, L. and Barnea, D., The relation between the Taylor bubble motion and the velocity field ahead of it, *Int. J. Multiph. Flow*, Vol.25, 1999, pp.957-975.

[18] Huzyak, P.C. and Koelling, K.W., The penetration of a long bubble through a viscoelastic fluid in a tube, *J. Non-Newton. Fluid Mech.*, Vol.71, 1997, pp.73-88.

[19] Gauri, V., Koelling, K. W., Gas-assisted displacement of viscoelastic fluids: flow dynamic at the bubble front, *J. Non-Newton. Fluid Mech.*, Vol.83, 1999, pp.183-203.

[20] Giavedoni, M. D. and Saita, F. A., The axisymmetric and plane cases of a gas phase steadily displacing a Newtonian liquid: A simultaneous solution of the governing equations, *Phys. Fluids*, Vol.9, 1997, pp.2420-2428.

[21] Giavedoni, M. D. and Saita, F. A., The rear meniscus of a long bubble steadily displacing a Newtonian liquid in a capillary tube, *Phys. Fluids*, Vol.11, 1999, pp.786-794.

[22] Wong, Harris, Radke, C.J. and Morris, S., The motion of long bubbles in polygonal capillaries. *Part 1. Thin films, J. Fluid Mech.,* Vol.292, pp. 71-94.

[23] Wong, Harris, Radke, C.J. and Morris, S. 1995 The motion of long bubbles in polygonal capillaries. Part 2. Drag, fluid pressure and fluid flow, *J. Fluid Mech.*, Vol. 292, 1995, pp. 95-110.

[24] Liao, Q and Zhao, T.S. , Modeling of Taylor bubble rising in a vertical mini noncircular channel filled with a stagnant liquid, *Int. J. Multiph. Flow*, Vol.29, 2003, pp.411-434.

[25] Kamişli, F., Flow of a long bubble in a square capillary, *Chem. Eng. Process.*, Vol.42, 2003, pp. 351-363.

[26] Pitts, E., Penetration of gluid into a Hele-Shaw cell: The Saffman-Taylor experiment, *J. Fluid Mech.*, Vol.97, 1980, pp.53-64.

[27] C.H. Hsu, P.C. Chen, K.Y. Kung, C. Lai , Impact of the Ratio of Asymptotic Bubble Width to Radius of Circular Tube and Reynolds Number in a Gas Bubble Driven Flow, *J. CHEMICAL ENGINEERING SCIENCE*, Vol.60, 2005, pp. 5341-5355.

[28] C.H. Hsu, K.Y. Kung, P. C. Chen and S. D. Huang, The Gas-assisted Fluid Flow Expelled in Front of a Long Bubble in a Circular Tube, *Transactions of the CSME*, Vol.30, No.1, 2006, pp.7-17.

[29] Reinelt, D. A. and Saffman, P. G. The penetration of a finger into a viscous fluid in a channel and tube, *SIAM J. Sci. Stat. Comput.*, Vol.6, 1985, pp.542-561.

[30] Puangdownreong, Deacha, Sujitjorn, Sarawut, Image approach to system identification., *WSEAS Transactions on Systems.*, Vol. 5, no. 5, 2006, pp. 930-938.